



# Developing time-of-flight polarized neutron capability at the China Spallation Neutron Source

Long Tian<sup>1,2</sup> · Ahmed Salman<sup>1,2</sup> · Chu-Yi Huang<sup>1,2,3</sup> · Yu-Chen Dong<sup>1,2,3</sup> · Fan Ye<sup>1,2,4</sup> · Ze-Cong Qin<sup>1,2</sup> · Wolfgang Kreuzpaintner<sup>1,2</sup> · Jun-Pei Zhang<sup>1,2</sup> · Tian-Hao Wang<sup>1,2</sup> · Xin Tong<sup>1,2</sup>

Received: 7 February 2023 / Revised: 14 May 2023 / Accepted: 20 May 2023 / Published online: 6 October 2023

© The Author(s), under exclusive licence to China Science Publishing & Media Ltd. (Science Press), Shanghai Institute of Applied Physics, the Chinese Academy of Sciences, Chinese Nuclear Society 2023

## Abstract

Polarized neutrons play an indispensable role in neutron scattering research and have been incorporated into various neutron diffractometers and spectrometers. Recognizing the importance of polarized neutrons, the China Spallation Neutron Source (CSNS) has dedicated resources for developing its own capabilities for polarized neutron techniques. Hence, a polarized neutron development platform was allocated to the BL-20 beam port at CSNS for the purpose of facilitating new technological developments and calibration of instruments. Here, we report the progress we have made in terms of using the established development platform at BL-20, including the characterization of neutron spin filter cells manufactured at CSNS, the calibration of self-developed polarized neutron instruments, performance of the polarized neutron technique applied to beamlines, and associated simulation work for beamline magnetic field environments. These results demonstrate the capability of the CSNS to develop time-of-flight polarized neutron instruments and techniques in-house, which will be incorporated into the construction of CSNS neutron beamlines.

**Keywords** Polarized neutron · Polarization analysis · Neutron instrumentation

This research was initiated and supported by the National Key Research and Development Program of China (No. 2020YFA0406000) and the National Natural Science Foundation of China (Nos. 12075265 and U2032219). The <sup>3</sup>He spin filter implemented in the experiment was developed as part of the Scientific Instrument Development Project of the Chinese Academy of Sciences (No. ZDKYYQ20190004), and Dongguan Introduction Program of Leading Innovative and Entrepreneurial Talents (No. 20191122). The magnetic field simulation and analysis were supported by Guangdong Natural Science Funds for Distinguished Young Scholars and the Guangdong Basic and Applied Basic Research Foundation (No. DG22311526).

✉ Tian-Hao Wang  
wangtianhao@ihep.ac.cn

✉ Xin Tong  
tongxin@ihep.ac.cn

Long Tian  
tianlong@ihep.ac.cn

<sup>1</sup> Institute of High Energy Physics, Chinese Academy of Science, Beijing 100049, China

## 1 Introduction

By taking advantage of the fact that neutrons are uncharged, yet possess magnetic moments, the polarized neutron technique has been widely applied to various types of neutron beamlines in major neutron sources worldwide. Applications of polarized neutrons stand out in research involving magnetic structures and excitations and are therefore prevalent in most neutron scattering experiments [1–4]. By utilizing polarized neutron techniques in diffraction research, contributions from nuclear, magnetic, and incoherent scattering can be identified, allowing the information about the magnetic structure obscured by other signals to be explicitly

<sup>2</sup> Spallation Neutron Source Science Center, Dongguan 523803, China

<sup>3</sup> School of Nuclear Science and Technology, University of the Chinese Academy of Sciences, Beijing 100049, China

<sup>4</sup> College of Materials Science and Engineering, Chongqing University, Chongqing 400044, China

separated, as demonstrated by applications at the Institut Laue-Langevin (ILL) D7 and the High Flux Isotope Reactor (HFIR) HB-1 [5–7]. In neutron spectroscopy experiments, neutron polarization analysis methods are used to distinguish magnons from phonons to study spin wave mechanisms. Typical applications of the polarized neutron spectrometry are performed at the ILL THALES and IN22 beamlines [8, 9]. For mesoscale and large-scale structural studies, the polarized neutron technique is commonly applied to neutron reflectometry and small-angle neutron scattering (SANS) beamlines, such as the beamlines of the Heinz-Maier-Leibnitz Zentrum (MLZ) KWS-1 and National Institute of Standards and Technology (NIST) NG-1 [10, 11].

The China Spallation Neutron Source (CSNS), designed as a large-scale multidisciplinary neutron source, currently operates with 100 kW proton beam power, generating a stable neutron beam with a high flux of neutrons. The CSNS provides a powerful and comprehensive research platform for many frontier disciplines involving the study of the structures and dynamics of various material systems [12–14]. Great demand exists for the capability to supply polarized neutrons to meet different research requirements at CSNS, including studies of nanomagnetic materials on its very small-angle neutron scattering spectrometer [15, 16], as well as magnetic dynamics studies of materials on the direct-geometry polarized neutron inelastic scattering spectrometer [17, 18]. In this case, in-house research and development (R&D) work on the polarized neutron technique is urgently needed for CSNS because commercially available polarized neutron components are often inadequate for customization, particularly for complex neutron beamline applications.

R & D in scientific instrumentation is crucial for maintaining the long-term performance and capabilities of a neutron beamline. Therefore, dedicated test beamlines are commissioned at neutron facilities, such as the NOBORU beamline at J-PARC in Japan [19], the TBL beamline at the European Spallation Source (ESS) in Sweden [20], and the HB-2D and CG-4B beamlines at HFIR in the USA. These beamlines support studies such as detector trials, polarized neutron imaging tests, examinations of instruments developed in-house, and verification of new techniques. The development of key instruments on test beamlines, including the calibration of  $^3\text{He}$  spin-filtering cells, detector tests, and examination of the chopper design [20–22], indicates the importance of development tests in the smooth commissioning of such instruments or techniques. In addition, these beamlines have contributed to advanced neutron research [23, 24].

The primary R & D goal for polarized neutrons at CSNS is to generate and manipulate polarized neutrons in a self-sufficient way. Significant progress has been made in this area, including the in-house development of  $^3\text{He}$  neutron spin filter (NSF) systems, neutron spin flippers, and customized guide field systems. As a newly commissioned neutron

source, CSNS also takes advantage of the opportunity to open up novel neutron experimental methods and further promote research on neutron methodology. To satisfy the in-house requirements for polarized neutron development, as well as to explore new techniques, time-of-flight polarized neutron development at CSNS aims to achieve quantitative analysis of neutron polarization across a wide range of wavelengths. Such work will be conducted under various beamline configurations along with customized simulations of the magnetic field environment and neutron polarization, which are expected to improve our understanding of the performance of polarized neutron setups.

In this paper, we report the performance of the polarized neutron technique under different combinations of customized polarized neutron instruments at the neutron technology development beamline (BL-20) at CSNS, as well as the capability of simulating the magnetic field environment and neutron polarization of the beamline, indicating that CSNS have the ability to generate and manipulate polarized neutron beams with high neutron polarization and transmission over a wide range of neutron wavelengths and can meet the needs of various neutron experiments.

## 2 Setup of the polarized neutron experiment platform at CSNS

Test experiments using polarized neutrons were conducted at BL-20. BL-20 uses a decoupled hydrogen moderator to slow down spallation neutrons at first, followed by a  $T_0$  chopper to filter out the high-energy flash at time 0, which is 11.4 ms away from the neutron beam port. By adjusting the phase of the  $T_1$  chopper mounted behind  $T_0$  with respect to the proton pulse, a bandwidth of 4.5 Å for a pulsed neutron beam was selected. In polarized neutron tests, typical wavelengths of 1–5.5 Å are selected to incorporate the pulse peak intensity while avoiding short-wavelength neutrons ( $\lambda < 1$  Å) that are naturally difficult to polarize. The spectrum within this bandwidth is shown in Fig. 1.

During the polarized neutron experiments at BL-20, four optical platforms were installed and coaligned using lasers in the beamline space. The neutron intensity spectrum was measured by using a time-of-flight  $^3\text{He}$  gas detector mounted at the end of the fourth platform. Another counter was mounted in front of the platform, near the beam port, as a beam monitor. Both the detector and monitor have their zero-time signals synchronized with the proton pulse to enable us to convert the neutron time of flight to its wavelength based on the following equation:

$$\lambda = \frac{2\pi}{k} = \frac{2\pi\hbar t}{mL}, \quad (1)$$

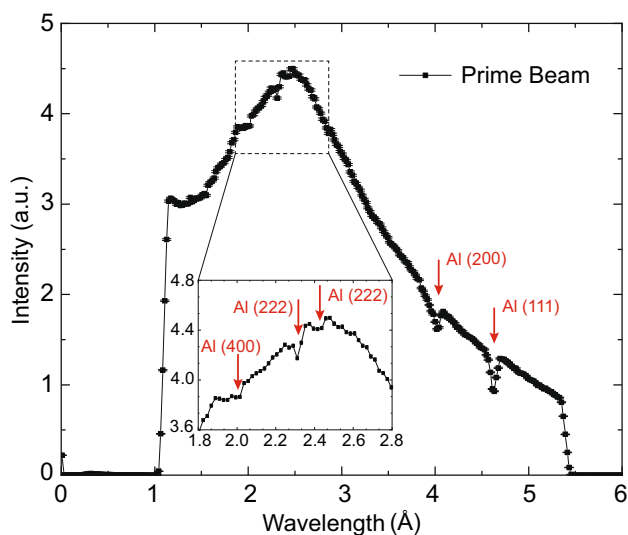


**Fig. 1** Prime beam profile provided at BL-20. The downward peaks in the profile curve represent the Bragg edges of aluminum

where  $m$  is the neutron mass,  $L$  is the distance between the moderator and detector,  $t$  is the time required for a neutron to travel between them,  $\hbar$  is the reduced Planck's constant. The wavelength was calibrated against the Bragg edges of aluminum, as indicated by the red arrows in Fig. 1. Initially, square neutron beams with a 12-mm length were produced. The beams were collimated using  $B_4C$  neutron slits of different sizes mounted along the neutron flight path.

The polarized neutron development platform at BL-20 was built by installing an arrangement of neutron spin polarizers, guide fields, spin manipulation devices, and final neutron spin analyzers before the detector. This platform was used to conduct polarized neutron experiments and perform quantitative neutron polarization analyses. Among the neutron spin polarizer and analyzer, at least one component is a polarized  $^3\text{He}$  spin filter device. A schematic layout of the experimental platform and corresponding photographic image of the equipment are shown in Fig. 2.

Benefiting from this development platform, multiple measurements for characterizing our customized neutron spin filter (NSF) cells, such as the cell pressure and lifetime of the  $^3\text{He}$  polarization, can be performed efficiently and accurately. In addition, our spin-exchange optical pumping (SEOP)-based  $^3\text{He}$  NSF systems were tested at BL-20 for stability and performance. Equipped with NSF cells with different characteristics, the  $^3\text{He}$  NSF systems were verified for their capacity to generate high neutron polarization over a wide range of neutron wavelengths, operate continuously and stably for a prolonged period, and implement spin flipping with lower  $^3\text{He}$  polarization losses [25–27]. Furthermore, neutron transmission measurements performed on this platform were used to test and characterize commercial

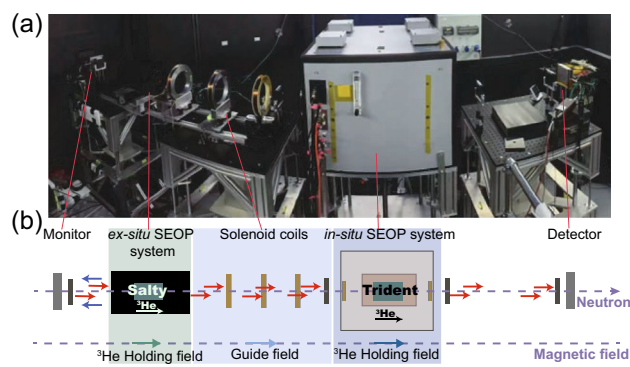


**Fig. 2** (Color online) **a** Photograph of the polarized neutron setup including the ex-situ and in-situ  $^3\text{He}$  NSF systems applied to BL-20. **b** Schematic diagram of the polarized neutron testing experiment corresponding to **a**. The blue and red arrows represent the different neutron spin polarizations, respectively, and the colored arrows at the bottom represent the magnetic field direction at corresponding regions

instruments such as a polarizing supermirror with a V-cavity. In combination with our in-house developed  $\pi$ -angle-reversal neutron spin flipper, which is a nonadiabatic fast passage spin flipper with ideal flipping efficiency, the calibrated supermirror can also yield polarized neutron beams with high polarization and can be utilized as polarizers or analyzers in future experiments.

In the following sections, we present our current achievements by applying the above neutron-polarizing instruments to the BL-20 development platform.

### 3 Neutron polarization testing result

Figure 2(a) shows the beamline configuration at BL-20, obtained by combining the ex-situ and in-situ  $^3\text{He}$  NSF systems for polarizing and analyzing incident neutron beams. This setup is more suitable for beamlines that have already been constructed, as they usually have a compact structure, or for experiments that require higher neutron polarization homogeneity over a wide wavelength range and mainly focus on studies within a lower wavelength range. Owing to the flexibility of the ex-situ  $^3\text{He}$  system, it is possible to easily assemble or disassemble instruments at the beamline or to switch NSF cells of different characteristics to satisfy the experimental requirements for varying neutron wavelengths. Using four  $B_4C$  slits in the instrument layout shown in Fig. 2b, a collimated neutron beam with a diameter of 10 mm was generated. A horizontal guide field of approximately 10 Gauss was generated using three self-designed solenoid coils mounted behind the ex-situ system, ensuring that the neutron spin was not affected by precession [29]. Following its passage through the ex-situ spin filter,

as indicated by the red arrows in Fig. 2b, the horizontally polarized neutron beam was analyzed by the in-situ system in accordance with the  $^3\text{He}$  polarizing direction within the NSF cell. During the measurements at BL-20, two different sets of neutron transmission data were collected by flipping the  $^3\text{He}$  polarization through the adiabatic fast passage (AFP) installed on the ex-situ  $^3\text{He}$  NSF system, which was verified to be highly efficient, with a loss of approximately 0.5% of  $^3\text{He}$  polarization per AFP operation. The neutron transmittances are labeled as  $T_{++}$  and  $T_{--}$ , where + and - represent the  $^3\text{He}$  polarization of  $^3\text{He}$  NSF systems parallel or antiparallel to their holding-field directions. As shown in Fig. 3a, the maximum value of  $T_{++}$ , which corresponds to the high neutron flux spin state, exceeded 40%. The neutron polarization  $P_n$  is given by [30]:

$$P_n = \frac{T_{++} - T_{--}}{T_{++} + T_{--}} \quad (2)$$

The  $^3\text{He}$  NSF systems are equipped with the in-house produced NSF cells named Salty and Trident, the parameters of which are listed in Table 1. With this combination of  $^3\text{He}$  NSF instruments, over 90% of the neutron polarization above 3.1 Å and over 94% above 4 Å can be obtained (Fig 3a). A comparison of the neutron polarization curves measured at different times revealed that the decay of  $^3\text{He}$  polarization over time in the ex-situ system resulted in a reduction in neutron polarization by less than 1% at 4 Å after 14.5 h of measurement, demonstrating that the  $^3\text{He}$  NSF setup can be used as a reliable method to produce polarized neutron beams with reasonable polarization over a prolonged period.

Additionally, the ex-situ system is considered a good choice for characterizing newly produced NSF cells at BL-20. This system was used to individually test the two NSF cells on the beamline to perform neutron transmission measurements on the unpolarized and polarized new cells loaded inside its solenoid, as shown in Fig. 3b. The properties of one of the new cells made of GE180 glass were determined to be the following: pressure of  $2.046 \pm 0.002$  bar and  $^3\text{He}$  polarization of  $52.3\% \pm 0.1\%$ , which is close to the  $49.2\% \pm 0.1\%$   $^3\text{He}$  polarization determined by electron paramagnetic resonance (EPR) measurement. These

**Table 1** Parameters of the customized cylindrical  $^3\text{He}$  NSF cells, including the cell inner length  $l$  and inner diameter  $\phi$ ,  $^3\text{He}$  pressure  $p$  at 25 °C, maximum lifetime  $T_1$  and maximum saturated  $^3\text{He}$  polarization  $P_{^3\text{He}}$

Cell name	$l \times \phi$ (cm)	$p$ (bar)	$T_1$ (h)	$P_{^3\text{He}}$ (%)
Trident	$7.9 \times 7.2$	$1.58 \pm 0.01$	$202.9 \pm 1.6$	$74.4 \pm 0.1$
Salty	$8.6 \times 7.1$	$1.62 \pm 0.04$	$239.9 \pm 13.8$	$77.7 \pm 1.9$

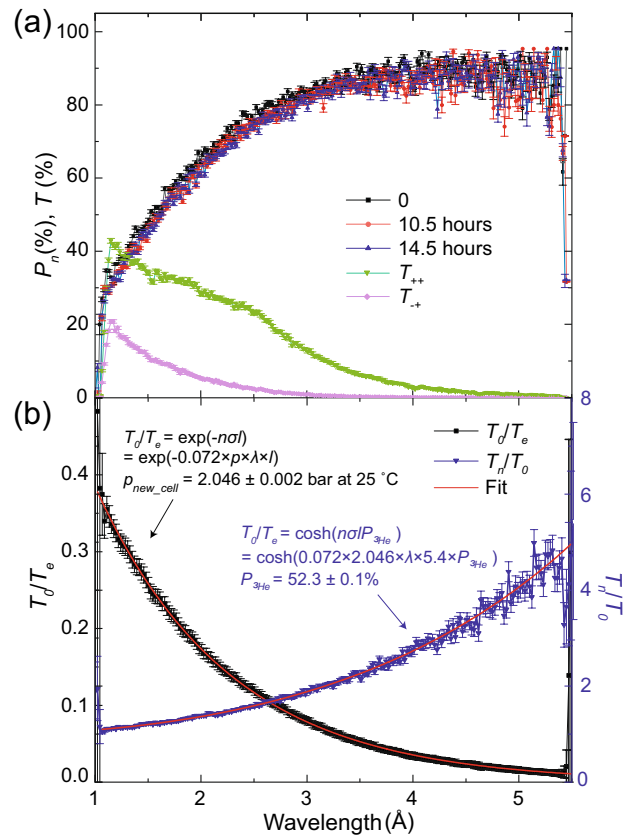


**Fig. 3** (Color online) **a** Neutron polarization and transmission measured with the setup shown in Fig. 2. The neutron polarization is plotted as a function of the neutron wavelength measured at different time, the transmission curves represent the high-flux spin state  $T_{++}$  and the low-flux spin state  $T_{--}$  corresponding to the measurements performed at the very beginning. **b** Neutron transmission data of one of the newly produced cells collected by using the ex-situ system individually. The transmission curves of the unpolarized cell and the transmission ratio of the polarized to the unpolarized cell are plotted in black and blue, respectively, where the cell pressure and  $^3\text{He}$  polarization can be derived from the fittings based on the equations labeled in the figure [27, 28].  $T_0$ ,  $T_n$ , and  $T_e$  are the neutron transmittance through depolarized, fully polarized, and empty  $^3\text{He}$  NSF cells, respectively,  $l$  is the cell inner length,  $n$  is the number density of the  $^3\text{He}$ ,  $\lambda$  is the neutron wavelength,  $\sigma = \sigma_0 \lambda$  with  $\sigma_0$  being the  $^3\text{He}$  absorption cross section for  $\lambda = 1$  Å  $p$  is the cell pressure, and  $P_{^3\text{He}}$  is the  $^3\text{He}$  polarization. The fitted values of the pressure and  $^3\text{He}$  polarization are 2.046 bar and 52.3%, respectively

results provide us with a reliable reference value to calibrate the results collected by offline nuclear magnetic resonance measurements.

Considering the figure of merit of a neutron polarization instrument, which is widely used as  $Q = P^2 T$  and is dependent on the neutron wavelength and beam angular width ( $\alpha$ ), the  $^3\text{He}$  NSF has its natural advantages in the research area requiring smaller  $\gamma$  and larger  $\alpha$  compared to polarizing supermirrors. This makes it more favorable for high-energy neutron scattering measurements with larger beam sizes,

such as off-specular neutron reflection measurements [31, 32]. In general, the performance of a polarizing supermirror is considered superior at longer wavelengths, since a much higher  $^3\text{He}$  polarization is required for the  $^3\text{He}$  NSF to counteract the rapid decrease in neutron transmittance and achieve a  $Q$  value comparable to that of a supermirror. Above the critical wavelength value, polarizing supermirrors have a large and constant neutron transmittance and polarization, and they perform independently of external influences.

At BL-20, to integrate the advantages of the  $^3\text{He}$  NSF and supermirror, extend the available wavelength range, and improve the  $Q$  of the entire beamline, we replaced the  $^3\text{He}$  NSF system with a combination of a polarizing supermirror and a neutron spin flipper as the incident beam polarizer and spin flipper, respectively. The polarizing supermirror installed behind the monitor, which consists of Si wafers coated on both sides with  $m = 4$  Fe/Si thin films, where  $m$  is a measure of critical angle in units of critical angle of nickel, was fabricated by SwissNeutronics and commissioned as a transmission geometry unit [33] (Fig. 4). The supermirror was assembled in a V-shape with a taper angle of  $1.19^\circ$  and mounted inside a magnetic casing with its field vertically aligned, which generated a critical wavelength of  $2 \text{ \AA}$ . Behind the supermirror, an in-house developed neutron spin flipper was employed to manipulate the neutron polarization and was verified to have polarization flipping efficiency of more than 90% and over 95% neutron transmittance at wavelengths longer than  $1.1 \text{ \AA}$  [34].

The main field directions between the supermirror polarizer and in-situ  $^3\text{He}$  NSF analyzer were different, and a customized guide field system was required to realize the

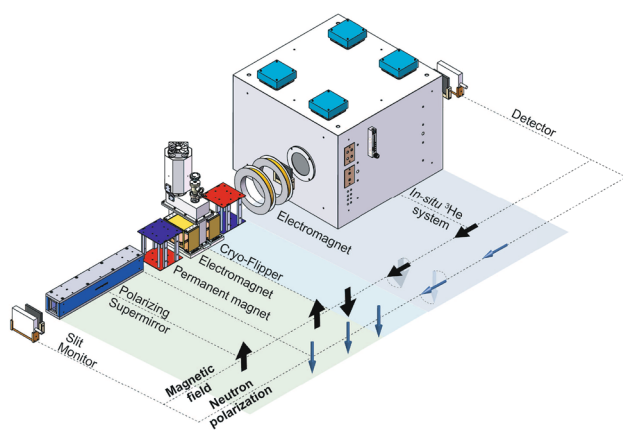


**Fig. 4** (Color online) Schematic diagram of the polarized neutron test experiment setup consisting of a supermirror, neutron spin flipper, in-situ  $^3\text{He}$  NSF system, the designed guide field system, and the neutron beam monitor and detector. The blue and black arrows represent the magnetic field and neutron evolution of the polarization along the central neutron trajectory, respectively

adiabatic transition of neutron polarization. Using the three-dimensional finite element method of the COMSOL Multiphysics<sup>®</sup> software [35], we simulated the magnetic field distribution along the overall beamline using calibrated models of the polarized neutron components. This led to the design of a suitable guide-field system. As shown in Fig. 5a, the field direction is initially along the vertical direction and

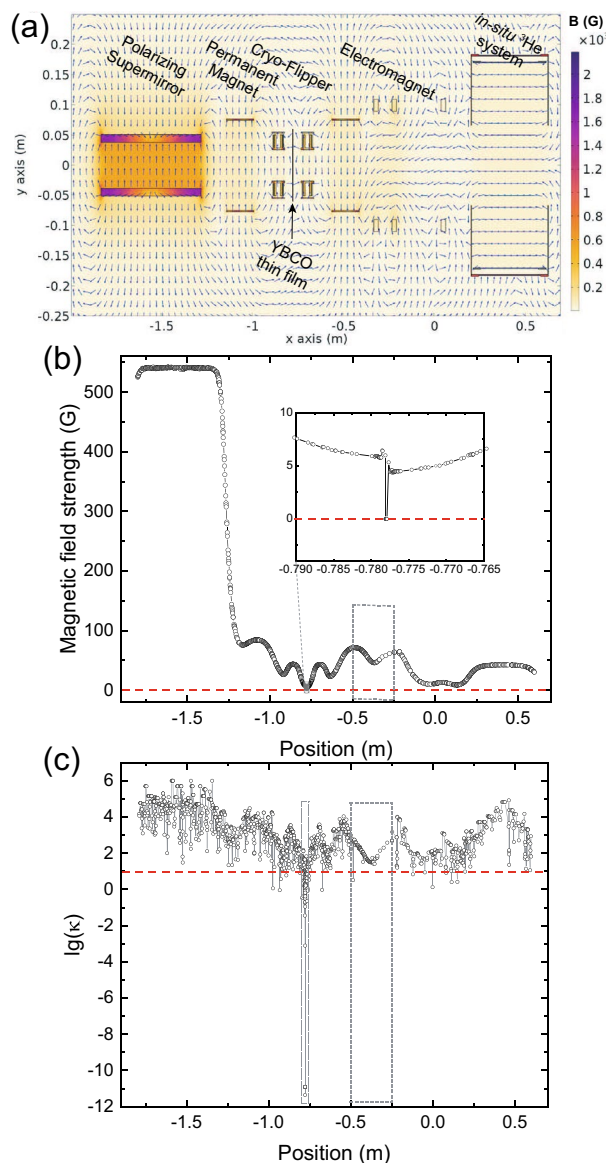


**Fig. 5** **a** Magnetic field simulation according to the beamline configuration shown in Fig. 4 using the finite element method. **b** One-dimensional cut of the magnetic field strength distribution along the center of the neutron trajectory. **c** Calculated adiabaticity parameter based on the field distribution shown in **b** for the  $2 \text{ \AA}$  neutrons. The dashed boxes in **b** and **c** represent the nonadiabatic transition area at the position of the yttrium barium copper oxide (YBCO) thin film and the adiabatic transition area between the guide field components, respectively

then becomes horizontally aligned between the permanent magnet and coil components. To satisfy the condition of adiabatic transition of the neutron polarization, the field strength and positions of all components were optimized along the entire neutron path (Fig. 5b). When determining the ability of the neutron spin to follow the magnetic field transitions along its trajectory, the evolution of the adiabaticity parameter ( $\kappa$ ) is always used as a reference. This parameter is defined as the ratio of the Larmor precession frequency  $\omega_L$  to the changing rate of magnetic field direction  $\omega_B$  [36],

$$\kappa = \frac{\omega_L}{\omega_B} = \frac{\gamma_n B}{d\theta_B/ds} \frac{m\lambda}{h}, \quad (3)$$

where  $\gamma_n$  is the neutron gyromagnetic ratio,  $h$  is Planck's constant,  $\theta_B$  is the angle of the magnetic field vector, and  $s$  is the distance travelled by neutrons. By applying the Bloch-Solver neutron-processing analysis software, as shown in Fig. 5c, the  $\kappa$  values at different positions were calculated based on the results of the magnetic field simulation. As represented by  $\kappa \ll 1$  ( $\lg(\kappa) \ll 0$ ) at the position of the neutron spin flipper, the flipping process is proven to be nonadiabatic. By contrast, for other values,  $\kappa > 10$  ( $\lg(\kappa) > 1$ ) at the other positions indicate the neutron polarization is preserved or manipulated adiabatically, particularly at the positions near the gap between the magnet and coil guide fields, where the neutron polarization was adjusted to be parallel to the  $^3\text{He}$  polarization. The beamline setup was constructed on the basis of the aforementioned simulations. The initial and final neutron polarization states were manipulated by adjusting the working status of the flipper and flipping the  $^3\text{He}$  polarization through AFP, and four neutron transmission measurements were performed. Their results are labeled  $T_{++}$ ,  $T_{--}$ ,  $T_{+-}$ , and  $T_{-+}$ , where the first index represents the flipper status and the second index represents the  $^3\text{He}$  polarization states. Hence, the overall beamline neutron polarization can be calculated using Eq. (2). The analyzing efficiency  $P_n(^3\text{He})$  of the  $^3\text{He}$  NSF system can also be determined independently from the neutron transmittances  $T_0$  and  $T_n$ , which can be given by [27, 28]

$$P_n(^3\text{He}) = \frac{T_+ - T_-}{T_+ + T_-} = \tanh(n\sigma l P_{^3\text{He}}) = \sqrt{1 - \frac{T_0^2}{T_n^2}}. \quad (4)$$

Additionally, a neutron polarization analysis method was applied to demonstrate that the flipping and polarizing efficiencies of the flipper and supermirror could be differentiated and derived from the above measurements. As indicated by the black curve in Fig. 6, the setup shown in Fig. 4 with the neutron spin flipper turned on and the  $^3\text{He}$  polarization flipped ( $T_{++}$  and  $T_{+-}$ ) is capable of providing effective neutron polarization. Furthermore, no obvious

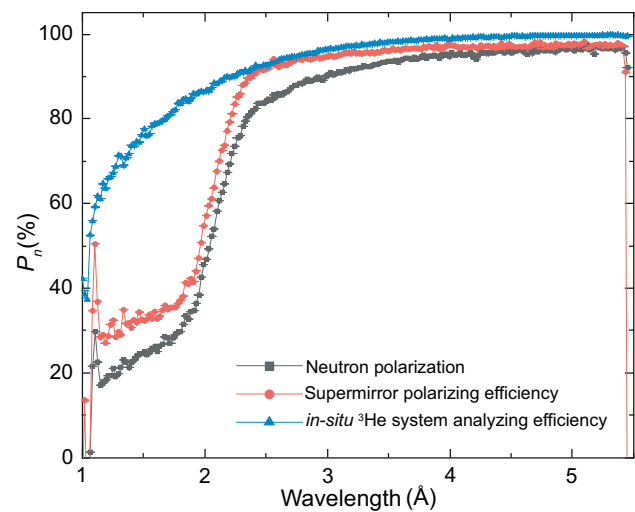


**Fig. 6** (Color online) Neutron polarization plotted as a function of the neutron wavelength. The black curve represents the neutron polarization of the overall beamline setup shown in Fig. 4. The blue curve represents the analyzing efficiency of the  $^3\text{He}$  analyzer, obtained from the neutron transmission measurements with an in-situ system. The red curve shows the polarizing efficiency of the supermirror polarizer determined from the neutron polarization of the beamline setup and the in-situ system

neutron polarization loss induced by the flipper or  $^3\text{He}$  AFP was observed in further measurements. The combination of the neutron polarization instruments listed above enabled a neutron polarization of more than 90% over 3 Å to be achieved, and the polarization at shorter wavelengths was improved to 50% at approximately 2 Å when the in-situ  $^3\text{He}$  NSF system was applied as an analyzer instead of the supermirror. The analysis efficiency of the in-situ  $^3\text{He}$  NSF system was calculated using equation (4) and is shown as the blue curve plotted in Fig. 6. Accordingly, the neutron polarization is 90% at 2.2 Å and reaches 99% at 4.1 Å. The red curve shows the derived polarizing efficiency of the supermirror used on BL-20, above its critical wavelength of 2 Å and the efficiency rapidly increases to reach more than 90% at 2.4 Å. Comparing the neutron polarization performances collected by different beamline setups, the performance of the  $^3\text{He}$  NSF polarizer surpasses that of the polarizing supermirror polarizer at wavelengths below approximately 2.3 Å, whereas the performance of the supermirror is more stable and consistent at longer wavelengths, which is in accordance with the characteristics of these components.

## 4 Conclusion

A new development platform for testing polarized neutron techniques with pulsed neutrons was verified at the neutron technology development beamline BL-20 at CSNS. Different combinations of polarized neutron instruments were used to assess the neutron beam polarization performance, including the utilization of  $^3\text{He}$  NSF systems as neutron spin polarizer and analyzer, as well as the replacement of the  $^3\text{He}$  NSF with a polarizing supermirror and neutron spin flipper to manipulate incident neutron polarization. Based on the design of the guide-field system supported by the simulation of the magnetic field, the neutron polarization of the former polarized neutron beam setup reached over 90% at 3.1 Å and was maximized at 94.5%, remaining stable within a difference of 1% over 14.5 h. The latter achieved neutron polarization of 50% at 2 Å, more than 90% over 3 Å, and maximum polarization of 96.5 %.

As evidenced by the diversity of the polarized-neutron setup at BL-20, the polarized neutron technique developed at CSNS is capable of supporting experiments with varied requirements in a wide range of research fields, and its feasibility makes it suitable for application to neutron beamlines at CSNS. Future developments aim to focus on improving the performance of the polarized neutron setup at BL-20 and the upcoming new testing beamline BL-8A, as well as the application to spectrometers that are currently under construction at CSNS that have corresponding requirements, such as the very small-angle neutron scattering spectrometer and the direct-geometry polarized inelastic spectrometer.

**Author Contributions** All authors contributed to the study conception and design. Material preparation, data collection and analysis were performed by Long Tian, Ahmed Salman, Chu-Yi Huang, Yu-Chen Dong, and Tian-Hao Wang. The first draft of the manuscript was written by Long Tian and all authors commented on previous versions of the manuscript. All authors read and approved the final manuscript.

**Data availability** The data that support the findings of this study are openly available in Science Data Bank at <https://doi.org/10.57760/sciencedb.10330> and <https://doi.org/10.57760/sciencedb.10330>.

## Declarations

**Conflict of interest** The authors declare that they have no competing interests.

## References

- H.A. Mook, M. Yethiraj, G. Aeppli et al., Polarized neutron determination of the magnetic excitations in  $\text{YBa}_2\text{Cu}_3\text{O}_7$ . *Phys. Rev. Lett.* **70**, 3490 (1993). <https://doi.org/10.1103/PhysRevLett.70.3490>
- D. Givord, H.S. Li, F. Tasset, Polarized neutron study of the compounds  $\text{Y}_2\text{Fe}_{14}\text{B}$  and  $\text{Nd}_2\text{Fe}_{14}\text{B}$ . *J. Appl. Phys.* **57**, 4100 (1985). <https://doi.org/10.1063/1.334631>
- S. Tomiyoshi, Y. Yamaguchi, Magnetic structure and weak ferromagnetism of  $\text{Mn}_3\text{Sn}$  studied by polarized neutron diffraction. *J. Phys. Soc. Jpn.* **51**, 2478–2486 (1982). <https://doi.org/10.1143/JPSJ.51.2478>
- Y. Nambu, J. Barker, Y. Okino et al., Observation of magnon polarization. *Phys. Rev. Lett.* **125**, 027201 (2020). <https://doi.org/10.1103/PhysRevLett.125.027201>
- T. Fennell, P.P. Deen, A.R. Wildes et al., Magnetic coulomb phase in the spin ice  $\text{Ho}_2\text{Ti}_2\text{O}_7$ . *Science* **326**, 415–417 (2009). <https://doi.org/10.1126/science.1177582>
- L. Mangin-Thro, Y. Sidis, A. Wildes et al., Intra-unit-cell magnetic correlations near optimal doping in  $\text{YBa}_2\text{Cu}_3\text{O}_{6.85}$ . *Nat. Comm.* **6**, 7705 (2015). <https://doi.org/10.1038/ncomms8705>
- T. Berlijn, P.C. Snijders, O. Delaire et al., Itinerant antiferromagnetism in  $\text{RuO}_2$ . *Phys. Rev. Lett.* **118**, 077201 (2017). <https://doi.org/10.1103/PhysRevLett.118.077201>
- D. Senff, P. Link, K. Hradil et al., Magnetic excitations in multi-ferroic  $\text{TbMnO}_3$ : evidence for a hybridized soft mode. *Phys. Rev. Lett.* **98**, 137206 (2007). <https://doi.org/10.1103/PhysRevLett.98.137206>
- P. Liu, M.L. Klemm, L. Tian et al., In-plane uniaxial pressure-induced out-of-plane antiferromagnetic moment and critical fluctuations in  $\text{BaFe}_2\text{As}_2$ . *Nat. Comm.* **11**, 5728 (2020). <https://doi.org/10.1038/s41467-020-19421-5>
- Z. Fu, Y. Xiao, A. Feoktystov et al., Field-induced self-assembly of iron oxide nanoparticles investigated using small-angle neutron scattering. *Nanoscale* **8**, 18541–18550 (2016). <https://doi.org/10.1039/C6NR06275J>
- K.V. O'Donovan, J.A. Borchers, C.F. Majkrzak et al., Pinpointing chiral structures with front-back polarized neutron reflectometry. *Phys. Rev. Lett.* **88**, 067201 (2002). <https://doi.org/10.1103/PhysRevLett.88.067201>
- H. Chen, X. Wang, China's first pulsed neutron source. *Nat. Mater.* **15**, 689–691 (2016). <https://doi.org/10.1038/nmat4655>
- J. Wei, S. Fu, J. Tang et al., China spallation neutron source—an overview of application prospects. *Chin. Phys. C* **33**, 1033 (2009). <https://doi.org/10.1088/1674-1137/33/11/021>
- J. Tang, Q. An, J. Bai et al., Back-n white neutron source at CSNS and its applications. *Nucl. Sci. Tech.* **32**, 11 (2021). <https://doi.org/10.1007/s41365-021-00846-6>
- Z. Fu, Y. Xiao, A. Feoktystov et al., Field-induced self-assembly of iron oxide nanoparticles investigated using small-angle neutron scattering. *Nanoscale* **8**, 18541–18550 (2016). <https://doi.org/10.1039/C6NR06275J>
- T. Köhler, A. Feoktystov, O. Petravic et al., Mechanism of magnetization reduction in iron oxide nanoparticles. *Nanoscale*, **13**, 6965–6976 (2021)
- J. Zhao, F.C. Niestemski, S. Kunwar et al., Electron-spin excitation coupling in an electron-doped copper oxide superconductor. *Nat. Phys.* **7**, 719–724 (2011). <https://doi.org/10.1038/nphys2006>
- H. Luo, M. Wang, C. Zhang et al., Spin excitation anisotropy as a probe of orbital ordering in the paramagnetic tetragonal phase of superconducting  $\text{BaFe}_{1.904}\text{Ni}_{0.096}\text{As}_2$ . *Phys. Rev. Lett.* **111**, 107006 (2013). <https://doi.org/10.1103/PhysRevLett.111.107006>
- K. Oikawa, F. Maekawa, M. Harada et al., Design and application of NOBORU-NeutrOn beam line for observation and research use at J-PARC. *Nucl. Instr. Meth. A.* **589**, 310–317 (2008). <https://doi.org/10.1016/j.nima.2008.02.019>
- R. Woracek, T. Hofmann, M. Bulat et al., The test beamline of the European spallation source - instrumentation development and wavelength frame multiplication. *Nucl. Instr. Meth. A.* **839**, 102–116 (2016). <https://doi.org/10.1016/j.nima.2016.09.034>

21. X. Jiang, J. Zhou, H. Luo et al., A large-area  $^3\text{He}$  tube array detector with vacuum operation capacity for the SANS instrument at CSNS. *Nucl. Sci. Tech.* **33**, 89 (2022). <https://doi.org/10.1007/s41365-022-01067-1>
  22. T. Okudaira, T. Oku, T. Ino et al., Development and application of a  $^3\text{He}$  Neutron Spin Filter at J-PARC. *Nucl. Instr. Meth. A.* **977**, 164301 (2020). <https://doi.org/10.1016/j.nima.2020.164301>
  23. M. Harada, M. Teshigawara, M. Ooi et al., Experimental characterization of high-energy component in extracted pulsed neutrons at the J-PARC spallation neutron source. *Nucl. Instr. Meth. A.* **1000**, 165252 (2021). <https://doi.org/10.1016/j.nima.2021.165252>
  24. Y. Kamiya, T. Miyoshi, H. Iwase et al., Development of a neutron imaging sensor using INTPIX4-SOI pixelated silicon devices. *Nucl. Instr. Meth. A.* **979**, 164400 (2020). <https://doi.org/10.1016/j.nima.2020.164400>
  25. C. Huang, J. Zhang, F. Ye et al., Development of a spin-exchange optical pumping-based polarized  $^3\text{He}$  system at the china spallation neutron source (CSNS). *Chinese Phys. Lett.* **9**, 092801 (2021). <https://doi.org/10.1088/0256-307X/38/9/092801>
  26. Z. Qin, C. Huang, Z.N. Buck et al., Development of a  $^3\text{He}$  gas filling station at the China spallation neutron source. *Chin. Phys. Lett.* **38**, 052801 (2021). <https://doi.org/10.1088/0256-307X/38/5/052801>
  27. J. Zhang, C. Huang, Z. Qin et al., In situ optical pumping for polarizing  $^3\text{He}$  neutron spin filters at China spallation neutron source. *Sci. China Phys. Mech.* **65**, 4 (2022). <https://doi.org/10.1007/s11433-021-1876-0>
  28. M. Batz, S. Baeßler, W. Heil et al.,  $^3\text{He}$  spin filter for neutrons. *J. Res. Natl. Inst. Stand. Technol.* **110**, 293–298 (2005). <https://doi.org/10.6028/jres.110.042>
  29. M. R. Fitzsimmons and C.F. Majkrzak, *Modern Techniques for Characterizing Magnetic Materials*, First edn. (MA: Kluwer Academic Publishers, Boston, 2005), pp. 44–47
  30. A. Salman, J. Zhou, J. Yang et al., Development of Time-of-Flight polarized neutron imaging at the China Spallation Neutron Source. *Chin. Phys. Lett.* **39**, 062901 (2022). <https://doi.org/10.1088/0256-307X/39/6/062901>
  31. F. Radua, A. Vorobiev, J. Major et al., Spin-resolved off-specular neutron scattering from magnetic domain walls using the polarized  $^3\text{He}$  gas spin filter. *Phys. B* **335**, 63–67 (2003). [https://doi.org/10.1016/S0921-4526\(03\)00192-3](https://doi.org/10.1016/S0921-4526(03)00192-3)
  32. V. Lauter-Pasyuk, H.J. Lauter, G.P. Gordeev et al., Nanoparticles in block-copolymer films studied by specular and off-specular neutron scattering. *Langmuir* **19**, 7783–7788 (2003). <https://doi.org/10.1021/la026818a>
  33. C. Schanzer, M. Schneider and P. Böni, Neutron optics: Towards applications for hot neutrons. *J. Phys. Conf. Ser.* **746**, 012024 (2016). <https://doi.org/10.1088/1742-6596/746/1/012024>
  34. Y. Dong, T. Wang, K. Wolfgang et al., Miniaturized time-of-flight neutron spin flipper using a high- $T_C$  superconductor. *Nucl. Sci. Tech.* **33**, 145 (2022). <https://doi.org/10.1007/s41365-022-01134-7>
  35. COMSOL AB, COMSOL Multiphysics @ v.6.0 cn.comsol.com. Stockholm, Sweden
  36. F. Bloch, Nuclear induction. *Phys. Rev.* **70**, 460–474 (1946). <https://doi.org/10.1103/PhysRev.70.460>
- Springer Nature or its licensor (e.g. a society or other partner) holds exclusive rights to this article under a publishing agreement with the author(s) or other rightsholder(s); author self-archiving of the accepted manuscript version of this article is solely governed by the terms of such publishing agreement and applicable law.